Enhanced Combined Tomography and Biomechanics Data for Distinguishing Forme Fruste Keratoconus

Allan Luz, MD; Bernardo Lopes, MD; Katie M. Hallahan, MD; Bruno Valbon, MD; Isaac Ramos, MD; Fernando Faria-Correia, MD; Paulo Schor, MD, PhD; William J. Dupps, Jr., MD, PhD; Renato Ambrósio, Jr., MD, PhD

ABSTRACT

PURPOSE: To evaluate the performance of the Ocular Response Analyzer (ORA) (Reichert Ophthalmic Instruments, Depew, NY) variables and Pentacam HR (Oculus Optikgeräte GmbH, Wetzlar, Germany) tomographic parameters in differentiating forme fruste keratoconus (FFKC) from normal corneas, and to assess a combined biomechanical and tomographic parameter to improve outcomes.

METHODS: Seventy-six eyes of 76 normal patients and 21 eyes of 21 patients with FFKC were included in the study. Fifteen variables were derived from exported ORA signals to characterize putative indicators of biomechanical behavior and 37 ORA waveform parameters were tested. Sixteen tomographic parameters from Pentacam HR were tested. Logistic regression was used to produce a combined biomechanical and tomography linear model. Differences between groups were assessed by the Mann–Whitney *U* test. The area under the receiver operating characteristics curve (AUROC) was used to compare diagnostic performance.

RESULTS: No statistically significant differences were found in age, thinnest point, central corneal thickness, and maximum keratometry between groups. Twenty-one parameters showed significant differences between the FFKC and control groups. Among the ORA waveform measurements, the best parameters were those related to the area under the first peak, p1area1 (AUROC, 0.717 ± 0.065). Among the investigator ORA variables, a measure incorporating the pressure-deformation relationship of the entire response cycle was the best predictor (hysteresis loop area, AUROC, 0.688 ± 0.068). Among tomographic parameters, Belin/Ambrósio display showed the highest predictive value (AUROC, 0.91 ± 0.057). A combination of parameters showed the best result (AUROC, 0.953 ± 0.024) outperforming individual parameters.

CONCLUSIONS: Tomographic and biomechanical parameters demonstrated the ability to differentiate FFKC from normal eyes. A combination of both types of information further improved predictive value.

[*J Refract Surg*. 2016;32(7):479-485.]

Corneal ectasia is one of the most feared complications of keratorefractive surgery, and there is interest in the preoperative identification of patients at risk for developing it.[1] Preoperative Placido disk-based topographic abnormalities for natural ectatic conditions, such as keratoconus, are considered the most important risk factor.[2] Despite well-defined clinical signs, the early forms of the disease present diagnostic challenges. The term "forme fruste keratoconus" (FFKC) refers to topographic patterns that are insufficient to reach the threshold of keratoconus based on computed quantitative indices.[3]

Recent advances in anterior segment tomography, based on Scheimpflug technology, have provided a variety of quantitative indices, such as detailed corneal pachymetry and elevation maps.[4,5] Studies have demonstrated that they can provide useful information in refractive screening.[6] Additionally, a panel of candidate diagnostic variables using exported Ocular Response Analyzer (ORA) (version 2.04; Reichert Ophthalmic Instruments, Depew, NY) data to characterize the temporal, applanation signal intensity, and pressure features of the corneal response demonstrated the ability to distinguish keratoconus from normal corneas more accu-

From the Department of Ophthalmology of the Federal University of São Paulo, São Paulo, Brazil (AL, PS, RA); Cole Eye Institute, Cleveland Clinic, Cleveland, Ohio (KMH, WJD); Biomedical Engineering, Cleveland Clinic Lerner Research Institute, Cleveland, Ohio (KMH, WJD); the Department of Ophthalmology of the University of São Paulo, São Paulo, Brazil (BV); Cornea and Refractive Surgery Department, Hospital de Olhos de Sergipe, Aracaju, Brazil (AL); Cornea and Refractive Surgery Department, Hospital de Braga, Braga, Portugal (FF-C); Rio de Janeiro Corneal Tomography and Biomechanics Study Group (AL, BL, BV, IR, FF-C, RA), Rio de Janeiro, Brazil; and Instituto de Olhos Renato Ambrósio and Visare Personal Laser, Rio de Janeiro, Brazil (BL, BV, RA).

Submitted: August 21, 2015; Accepted: March 17, 2016

Supported in part by NIH R01EY023381 (WJD).

Dr. Ambrósio is a consultant for Oculus Optikgeräte GmbH (Wetzlar, Germany). Dr. Dupps has intellectual property issued through Cleveland Clinic Innovations for a technique for biomechanical measurement that is not addressed in this article, is a consultant for Ziemer, and is on the sponsored research and medical advisory board for Avedro. The remaining authors have no financial or proprietary interest in the materials presented herein.

Correspondence: Allan Luz, MD, Jorge Amado Avenue, 1500 – Jardins – 49025 330 Aracaju, SE – Brazil. E-mail: dr.allanluz@gmail.com

doi:10.3928/1081597X-20160502-02

rately than some original pressure-derived parameters[7] (corneal hysteresis [CH] and corneal resistance factor [CRF]).

The purpose of this study was to evaluate the diagnostic capacity of tomographic parameters, ORA biomechanical variables (including novel waveform-derived variables related to pressure, applanation signal intensity, response time, and combinations of these variables), and a combination model in differentiating FFKC from normal corneas.

PATIENTS AND METHODS

This study was a comparative, observational, retrospective, non-interventional case series. It was approved by the Ethics and Research Committee of São Paulo Federal University (Protocol 2012/10) and followed the tenets of the Declaration of Helsinki.

Patients were examined at the Instituto de Olhos Renato Ambrósio (Rio de Janeiro, Brazil). We studied 97 eyes of 97 patients who were divided into two groups: the FFKC group, comprising 21 eyes of 21 patients with normal Placido-disk corneal topographies and in whom the fellow eye had keratoconus, and the control group, comprising 76 eyes of 76 patients with bilateral normal corneas (**Figure A**, **Figure B**, and **Figure C**, available in the online version of this article). The control group was formed by randomly choosing a single eye of patients with bilaterally normal eyes according to topographic criteria.

The criteria of normality and disease were based on the Rabinowitz indices and were evaluated by a corneal topographer using Placido disks (Atlas 9000; Carl Zeiss Meditec, Jena, Germany). A KISA index greater than 100% was considered early keratoconus, less than 60% was considered normal, and 60% to 100% was considered suspected keratoconus.[8] The fellow eye was considered for analysis when the KISA index on corneal topography was less than 60% without a suspect pattern.

The control group included patients without corneal topographic irregularities, high refractive error, or collagen vascular disease. Excluded from both groups were patients with severe atopic keratoconjunctivitis,[9] a history of ocular surgery or any eye disease, except for keratoconus in the fellow eye of patients with FFKC, or any systemic disease or syndrome.

A comprehensive eye examination was conducted for all patients. In addition to topographic data, the following information was obtained for each patient: age, thinnest point, central corneal thickness, topographic astigmatism, and maximum keratometry (Kmax). Biomechanical data were obtained with the ORA and included the Goldmann-correlated intraocular pressure (IOPg), corneal compensated intraocular pressure (IOPcc), CH, CRF, 37 parameters derived from analyses of the waveform signal,[10] and 15 custom variables proposed in this article using exported ORA data to characterize the temporal, applanation signal intensity, and pressure features of the corneal response. Additionally, 16 tomographic parameters from the Pentacam HR Scheimpflug tomography system (Oculus Optikgeräte GmbH, Wetzlar, Germany) were tested. The following were derived from the corneal surface: index surface variance, index of vertical asymmetry, and index of height decentration. The following were derived from elevation: enhanced best fit sphere (BFS) front, enhanced BFS back, elevation B BFS Apex, elevation B BFS Thinnest, elevation B BFS Max 4-mm Zone, elevation B best fit toric ellipsoid (BFTE) Apex, elevation B BFTE Thinnest, and elevation B BFTE Max 4-mm Zone. The following were derived from pachymetry: Belin/Ambrósio display (BAD-D), Ambrósio relational thickness (ART) Max, ART Average, relative pachymetric increase (RPI) Max, and RPI Average. Elevation data were taken from a fixed 8-mm zone (BFS set to manual, float, sphere, diameter 8 mm) centered on the corneal apex. All tomographic variables and their interpretations are described in **Table A** (available in the online version of this article).

ORA infrared intensity and pressure time series data were exported using ORA software and analyzed using custom Matlab routines (version 7.0; MathWorks, Natick, MA) as described previously.[7] Briefly, 15 variables were derived from the ORA signal and grouped according to waveform features: applanation signal intensity (group 1), applied pressure (group 2), time (group 3), the applanation signal intensity as a function of response time (group 4), the relationship between applied pressure and the applanation signal response (group 5), and the relationship between pressure and time (group 6). All variables and their interpretations are described in **Table B** (available in the online version of this article). These investigator-derived variables defined features from the ORA signal are hypothesized to be biomechanically relevant[7]; they are introduced in **Figure 1**.

The ORA calculates a waveform score that is used to select the best quality measurement value of each parameter.[11] We used the examination with the best waveform score (ie, the best quality measurement) after four consecutive measurements. All ORA and Pentacam data were obtained by the same experienced operator (BV) in a consistent way during office hours.

Statistical analyses were performed using BioEstat 5.0 (Mamirauá Institute, Amazonas, Brazil) and MedCalc 11.1 (MedCalc Software, Mariakerke, Belgium) software. The non-parametric Mann–Whitney *U* test (Wilcoxon rank sum) was used to evaluate the distribu-

tion of variables between the two groups. The significance criterion was subjected to Bonferroni correction.

The receiver operating characteristics (ROC) curve and the area under the ROC curve (AUROC) were calculated for each parameter to examine differences between the groups and determine the overall predictive accuracy of each test. The standard error of the AUROC was evaluated using the method of DeLong et al.[12] The exact binomial method was used to calculate confidence intervals for AUROCs, with 0.700 indicating the cut-off point for poor parameter performance.[10] Nonparametric pair-wise comparisons of the ROC curves were performed to test whether significant differences were present in the areas for each parameter using the Hanley–McNeil method for calculating the standard error.[13,14] *P* values less than .05 were considered statistically significant. The results are expressed as AUROC, sensitivity, and specificity. In **Table C** (available in the online version of this article), the AUROC, *P* value, sensitivity, specificity, confidence interval, standard error, and cut-off values are presented.

Furthermore, step-wise logistic regression analysis[15] was performed to combine the best variables from ORA-derived biomechanical properties and Pentacam-derived tomographic parameters to determine the predictive capability (function-enhanced combined tomography and biomechanics [FECTB]). Based on the control and FFKC groups, the discriminant analysis resulted in a linear function of the variables:

$$L = b_1x_1 + b_2x_2 + b_nx_n + c$$

where b is a discriminant coefficient, x is an input variable, and c is a constant.

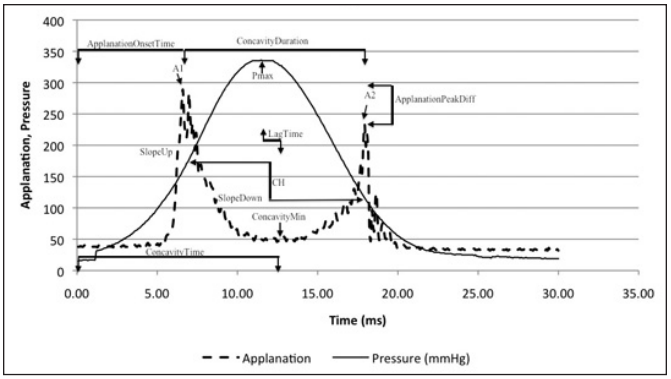

Figure 1. Ocular Response Analyzer (ORA) (Reichert Ophthalmic Instruments, Depew, NY) signal output with select variables from applanation signal intensity (A1, A2, Applanation peak difference, and Concavity min); pressure (Pmax); time (concavity duration, concavity time, and lag time); applanation signal intensity as a function of response time (slope up and slope down). CH = corneal hysteresis

RESULTS

Table 1 summarizes the demographic, IOP, and topographic and tomographic characteristics of each group. Mean central pachymetry, thinnest point of the cornea, age, IOPg, IOPcc, astigmatism, and Kmax were not significantly different between the groups ($P > .05$). The mean KISA index was 17.87% in the FFKC group and 11.57% in the control group ($P = .049$).

Table D (available in the online version of this article) compares the biomechanical parameters of the groups. Eleven parameters differed significantly between the groups: Pmax ($P = .391$), hysteresis loop area (HLA) ($P = .0086$), Impulse ($P = .0363$), p1area ($P = .0037$), dive1 ($P = .0375$), h1 ($P = .0228$), p1area1 ($P = .0024$), h11 ($P = .0228$), uslope2 ($P = .0478$), mslew2 ($P = .0421$), and slew2 ($P = .0487$) (**Table 2**). Neither CH nor CRF showed a statistically significant difference.

TABLE 1
Comparison of Characteristics and Intraocular Pressure

Characteristic	FFKC Group Mean ± SD (Range)	Control Group Mean ± SD (Range)	*P*[a]
Patients	21	76	–
Eyes	21	76	–
Age (y)	25.5 ± 7.2 (14.9 to 48.5)	25.7 ± 5.2 (12.5 to 38.8)	.50
Central pachymetry (μm)	527.3 ± 16.7 (477 to 576)	530 ± 26.3 (458 to 632)	.05
Thinnest point (μm)	526 ± 16.9 (474 to 566)	527.4 ± 26 (457 to 629)	.10
Astigmatism (D)	1.20 ± 0.80 (0.20 to 3.40)	1.50 ± 1.10 (0.10 to 5.30)	.30
Kmax (D)	44.90 ± 1.80 (42.30 to 48.40)	44.40 ± 1.40 (400 to 47.70)	.50
IOPg (mm Hg)	12.5 ± 2.8 (8.4 to 17.2)	13.8 ± 2.9 (7.9 to 20)	.10
IOPcc (mm Hg)	14.3 ± 3.4 (9.9 to 21)	14.8 ± 2.6 (7.6 to 21.7)	.30

FFKC = forme fruste keratoconus; SD = standard deviation; D = diopters; Kmax = maximum keratometry; IOPg = Goldmann intraocular pressure; IOPcc = corneal compensate intraocular pressure
[a]*Mann–Whitney U test.*

TABLE 2
Comparison of ORA Variables With the Best 11 Parameters Differing Significantly Between the Groups

Parameter	Normal Mean ± SD (Range)	FFKC Mean ± SD (Range)	P[a]
p1area1	1,412.29 ± 447.54 (554.25 to 2,686.5)	1,085.19 ± 363.43 (553.5 to 1,762.38)	.0024[b]
p1area	3,331.25 ± 910.23 (1,402 to 5,606.06)	2,644.83 ± 746.93 (1,450.13 to 4,008)	.0037[b]
HLA	5,501.00 ± 15,339.15 (8,853 to 97,693)	4,3614.55 ± 18,597.56 (-11,656.5 to 78,052)	.0086[b]
h1	377.05 ± 103.64 (218.62 to 640.87)	319.06 ± 102.74 (168.75 to 563.62)	.0228[b]
h11	251.37 ± 69.09 (145.75 to 427.25)	212.70 ± 68.49 (112.5 to 375.35)	.0228[b]
Impulse	4,536.22 ± 323.30 (3,775.35 to 5,314.08)	4,402.86 ± 418.84 (3,796.58 to 5,807.36)	.0363
dive1	323.77 ± 117.79 (38.75 to 614.5)	266.39 ± 115.82 (19.5 to 561.75)	.0375
Pmax	423.74 ± 35.49 (344 to 505)	408.43 ± 45.09 (348 to 557)	.0391
mslew2	127.75 ± 56.57 (25.75 to 326)	97.08 ± 51.35 (19.25 to 173)	.0421
uslope2	85.99 ± 43.24 (14.67 to 239.12)	62.14 ± 45.55 (3.27 to 138.75)	.0478
slew2	86.40 ± 42.63 (17.5 to 239.12)	63.70 ± 44.10 (6.66 to 138.75)	.0487

ORA = Ocular Response Analyzer (Reichert Ophthalmic Instruments, Depew, NY); SD = standard deviation; FFKC = forme fruste keratoconus
[a]*Mann-Whitney U test.*
[b]*Statistically significant difference after Bonferroni correction.*

TABLE 3
Comparison of Tomographic Parameters for Normal and FFKC Groups

Parameter	Normal Group Mean ± SD (Range)	FFKC Group Mean ± SD (Range)	P[a]
BAD-D	0.52 ± 0.50 (-0.68 to 1.34)	1.84 ± 1.34 (-0.22 to 7)	< .0001[b]
ART Maximum	497.90 ± 72.82 (403 to 663)	379.80 ± 88.49 (250 to 593)	< .0001[b]
ART Average	608.11 ± 78.86 (486 to 807)	495.04 ± 89.09 (329 to 718)	< .0001[b]
Elevation B BFS 8-mm Thinnest	1.52 ± 3.10 ((-3 to 9)	7.47 ±.5.65 (-5 to 18)	< .0001[b]
Elevation B BFTE 8-mm Thinnest	-1.44 ± 2.83 (-7 to 7)	3.95 ± 4.89 (-8 to 14)	< .0001[b]
Elevation B BFTE 8-mm Max 4-mm Zone	6.81 ± 2.01 (4 to 13)	9.57 ± 3.20 (18 to 4)	< .0001[b]
RPI Maximum	1.05 ± 0.16 (0.82 to 1.36)	1.41 ± 0.28 (0.91 to 1.94)	< .0001[b]
RPI Average	0.87 ± 0.10 (0.68 to 1.04)	1.03 ± 0.16 (0.73 to 1.47)	< .0001[b]
Enhanced BFS Front 8 mm	7.93 ± 0.22 (7.38 to 8.57)	7.81 ± 0.20 (7.44 to 8.1)	.0413
Elevation B BFTE 8-mm Apex	-1.31 ± 3.14 (-8 to 8)	0.80 ± 4.47 (-7 to 11)	.043
Enhanced BFS Back 8 mm	6.57 ± 0.22 (5.97 to 7.17)	6.47 ± 0.23 (6.05 to 6.86)	.1232
IHD	3.60 ± 2.28 (0.001 to 8)	4.85 ± 3.07 (0.001 to 8)	.1677
Elevation B BFS 8-mm Apex	0.78 ± 2.28 (-3 to 9)	2.23 ± 4.04 (-4 to 13)	.2217
ISV	21.32 ± 7.42 (46 to 8)	19.33 ± 5.23 (10 to 31)	.446
Elevation B BFS 8-mm Max 4-mm Zone	13.53 ± 4.63 (4 to 26)	14.52 ± 4.94 (7 to 27)	.4539
IVA	0.37 ± 1.17 9 (0.04 to 7)	0.16 ± 0.06 (0.09 to 0.3)	.6456

FFKC = forme fruste keratoconus, SD = standard deviation; BAD-D = Belin/Ambrósio display; ART = Ambrósio relational thickness; BFS = best fit sphere; BFTE = best fit toric ellipsoid; RPI = relative pachymetric increase; IHD = index of height decentration; ISV = index suface variance; IVA = index of vertical asymmetry
[a]*Mann–Whitney U test.*
[b]*Statistically significant difference after Bonferroni correction.*

Table 3 compares the tomographic parameters of groups. Ten of 16 parameters differed significantly between the groups: BAD-D ($P < .0001$), ART Max ($P < .0001$), ART Avg ($P < .0001$), enhanced BFS front ($P = .0413$), elevation B BFS Thinnest ($P < .0001$), elevation B BFTE Apex ($P = .043$), elevation B BFTE Thinnest ($P < .0001$), elevation B BFTE Max 4-mm Zone ($P < .0001$), and RPI Max and RPI avg ($P < .0001$).

Results of ROC analysis showed that the five best-performing variables, determined by the highest AUROC

values, were BAD-D (AUROC, 0.91), Elevation B BFTE Thinnest (AUROC, 0.872), ART Max (AUROC, 0.863), RPI Max (AUROC, 0.841), and Elevation B BFS Thinnest (AUROC, 0.0839). BAD-D, Elevation B BFTE Thinnest, and ART Max showed sensitivities of 90.48%, 85.71%, and 85.71% and specificities of 82.89%, 78.95%, and 78.95%, respectively (**Table C**).

Moreover, the highest AUROC was found for the logistic regression model. Sensitivity was 85.71%, specificity was 98.68%, and the AUROC was 0.953. The regression was expressed by the following formula:

1.167 × BAD-D – 0.003 × ART Max – 1.758 × Enhanced BFS Front +0.141 × Elevation B BFTE Thinnest + 0.492 × Elevation B BFTE Max 4-mm Zone – 0.017 × Pmax -3.505 × HLA -2.705 × p1area -0.002 × dive1 – 0.020 × slew2

Additionally, **Figure 2** shows the AUROCs of FECTB, p1area1, and BAD-D. These parameters were the best from each group (tomography and biomechanics).

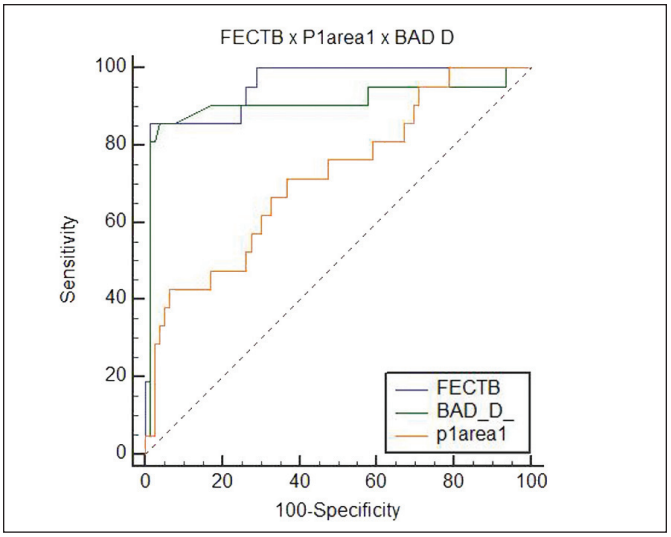

Figure 2. Receiver operating characteristic curves for function-enhanced combined tomography and biomechanics (FECTB), P1area1, and Belin/Ambrósio display (BAD_D).

DISCUSSION

The diagnostic approach for FFKC has improved in recent years, mainly due to contemporary anterior segment imaging technologies. Indices such as the ART and BAD-D facilitate the identification of corneal abnormalities.[1,5,16] Our study used these indices and others related to the elevation and pachymetry distribution to discriminate FFKC from normal corneas. Additionally, this study provides insight into differences in the dynamic behavior of FFKC and normal eyes through analysis of novel waveform-derived candidate variables related to pressure, applanation, response time, or a combination of these variables.[7]

Our study suggests that a combined tomography and biomechanical approach can enhance screening for FFKC. Although tomographic findings have shown better overall results, it was by combining them with biomechanical data that we determined the best AUROC to discriminate between the two groups. Taking into account that our groups are matched for thinnest point, Kmax, age, and central pachymetry values, there is no index in the "classic" screening that distinguishes between the two populations, and the differences found were derived from intrinsic characteristics of the cornea.[17]

FFKC shows (1) marked reductions in a comprehensive hysteresis analog (HLA) that captures the pressure deformation behavior of the entire response cycle, (2) reduction in the force and time required to reach initial applanation, (3) lower maximum air pressure intensity required to produce applanation as a function of a peak pressure and time, (4) reduced area under the initial applanation intensity curve, (5) no difference in high-frequency oscillation in regions between peaks and no difference from normal in corneal deformation after a puff, and (6) lower speed of corneal deformation after applanation. Likewise, parameters of pachymetry and elevation, such as BAD-D and ART Max, showed excellent results. These results suggest that FFKC is characterized by a modification of the cornea's shape and thickness. The highlight of the parameters derived from the back elevation at the thinnest point is BFTE or BFS, the AUROCs of which were 0.87 and 0.83, respectively, suggesting that an increase in posterior elevation concomitant to corneal thinning may be an important sign of FFKC.[18]

According to a previous study that assessed FFKC with Orbscan data, posterior elevation and corneal thickness indices may be the most useful parameters to discriminate between the FFKC and normal groups. The same study suggested that Placido disk-based indices were not sufficient to detect the earliest form of keratoconus.[18] Another study using the Pentacam, similar to our study, showed corneal thickness distribution and posterior elevation to be more helpful than anterior curvature data in identifying eyes with subclinical keratoconus.[19] As described previously, corneal thickness at the thinnest point, corneal thickness spatial profile, and percentage of thickness increase are known discriminant indices between keratoconus and normal.[4] Furthermore, ART values were shown to be better than single-point pachymetric parameters for discriminating normal eyes from keratoconic eyes.[5] A previous study found that anterior curvature data had a higher discriminant ability than elevation or pachymetric parameters, but this difference may be ex-

plained by differing methodologies, where FFKC was defined not with normal anterior curvature but with elevation and pachymetry using the BAD-D.[20]

Regarding the biomechanical indices, our results demonstrated that CH and CRF were not capable of discriminating FFKC (P = .13 and .08, respectively). A previous study differed from this,[21] probably because our group was more restrictive in morphological properties, being matched for thinnest point, Kmax, central pachymetry, and age. Our findings confirm prior results showing that maximum applied pressure levels were significantly different between FFKC and normal eyes, with lower values for FFKC.[17] In a previous study comparing the same custom variables in keratoconic and normal eyes, all variables except lag time were significantly different, and the concavity min and HLA showed the greatest discriminant value for keratoconus.[7] In the current study, HLA showed an AUROC of 0.688 (sensitivity 61.90%, specificity 61.84%) and was the best discriminant custom variable.

The concern that IOP differences could confound the predictive value of key variables in the current study was minimized due to absence of statistically significant IOPg or IOPcc differences between groups. Moreover, although the difference between the two groups was statistically significant (P = .049), KISA index values were far below the 60% threshold for classification as suspected keratoconus based on anterior topography features alone.[8]

Among all of the biomechanical parameters, those that showed the best outcomes were p1area and p1area1 (AUROC 0.707 and 0.717, respectively). A previous study also highlighted p1area, p1area1, p2area, and p2area1 for their performance in identifying grades I and II keratoconus.[22] By contrast, the current study demonstrated only that areas related to the first applanation event were significant in FFKC. Low values of p1 and p2 represent rapid applanation or applanation-recovery responses that are consistent with less viscous damping, but may also reflect reduced applanation signal intensities due to complex corneal surface deformation responses, driven by corneal material property inhomogeneities. Because the applanation signal height variables were significantly lower in the FFKC group in this study and the width was not significantly different, it seems likely that the lower mean applanation signal height was the driver of lower p1area in the FFKC group.

The main clinical importance of our findings is that a combination of parameters, biomechanical and tomographic, can achieve better results than the cited variables studied individually. Unlike other studies that studied only traditional CH and CRF, our study goes further and presents a wide range of biomechanical data beyond CH and CRF. Although elevation and pachymetric indices achieved better individual AUROC values when studied independently (BAD-D AUROC, 0.91 and ART Max AUROC, 0.863), the best outcome can be achieved with the introduction of biomechanical data (FECTB AUROC, 0.953).

Some characteristics and limitations of our study should be considered. First, our study is limited by the small number of participants in the FFKC group. Second, this study was an exploratory analysis designed to restrict the initial number of candidate variables to a smaller subset of promising variables. Third, other tomographic findings, such as corneal volume, were not studied because they have been shown not to undergo significant changes in the early stages of the disease.[23]

Pentacam HR tomographic parameters and ORA biomechanical custom variables can be useful in diagnosing FFKC. A combination of both types of information further improved the predictive value. Additional research on these models will contribute to validating software that may help the clinician in detecting susceptibility to corneal ectasia.

AUTHOR CONTRIBUTIONS

Study concept and design (AL, KMH, PS, WJD, RA); data collection (AL, BL, BV, IR, FF-C); analysis and interpretation of data (AL, KMH, WJD, RA); writing the manuscript (AL, BL, BV, IR, FF-C, PS); critical revision of the manuscript (KMH, WJD, RA); statistical analysis (BL); supervision (WJD, RA)

REFERENCES

1. Binder PS, Trattler WB. Evaluation of a risk factor scoring system for corneal ectasia after LASIK in eyes with normal topography. *J Refract Surg*. 2010;26:241-250.
2. Randleman JB, Trattler WB, Stulting RD. Validation of the Ectasia Risk Score System for preoperative laser in situ keratomileusis screening. *Am J Ophthalmol*. 2008;145:813-818.
3. Klyce SD. Chasing the suspect: keratoconus. *Br J Ophthalmol*. 2009;93:845-847.
4. Ambrósio R Jr, Alonso RS, Luz A, Coca Velarde LG. Corneal-thickness spatial profile and corneal-volume distribution: tomographic indices to detect keratoconus. *J Cataract Refract Surg*. 2006;32:1851-1859.
5. Ambrósio R Jr, Caiado AL, Guerra FP, et al. Novel pachymetric parameters based on corneal tomography for diagnosing keratoconus. *J Refract Surg*. 2011;27:753-758.
6. Belin MW, Villavicencio OF, Ambrósio RR Jr. Tomographic parameters for the detection of keratoconus: suggestions for screening and treatment parameters. *Eye Contact Lens*. 2014;40:326-330.
7. Hallahan KM, Sinha Roy A, Ambrósio R Jr, Salomao M, Dupps WJ Jr. Discriminant value of custom ocular response analyzer waveform derivatives in keratoconus. *Ophthalmology*. 2014;121:459-468.

8. Rabinowitz YS, Rasheed K. KISA% index: a quantitative videokeratography algorithm embodying minimal topographic criteria for diagnosing keratoconus. *J Cataract Refract Surg*. 1999;25:1327-1335.
9. Ibrahim OM, Dogru M, Kaido M, Kojima T, Fujishima H, Tsubota K. Functional visual acuity assessment of severe atopic keratoconjunctivitis. *Cornea*. 2014;33(suppl 11):S13-S18.
10. Mikielewicz M, Kotliar K, Barraquer RI, Michael R. Air-pulse corneal applanation signal curve parameters for the characterisation of keratoconus. *Br J Ophthalmol*. 2011;95:793-798.
11. Luz A, Fontes BM, Lopes B, Ramos I, et al. Best waveform score for diagnosing keratoconus. *Revista Brasileira de Oftalmologia*. 2013;72:361-365.
12. DeLong ER, DeLong DM, Clarke-Pearson DL. Comparing the areas under two or more correlated receiver operating characteristic curves: a nonparametric approach. *Biometrics*. 1988;44:837-845.
13. McNeil BJ, Hanley JA. Statistical approaches to the analysis of receiver operating characteristic (ROC) curves. *Med Decis Making*. 1984;4:137-150.
14. McNeil BJ, Kirkwood JR, Hanley JA, Polak J, Wilkinson R, Funkenstein HH. Computed tomographic studies of the head in a teaching hospital and a community hospital: a comparison. *Radiology*. 1982;145:367-370.
15. Hosmer DW Jr, Lemeshow S. *Applied Logistic Regression,* 2nd ed. New York: John Wiley & Sons; 2000.
16. Ambrósio R Jr, Ramos I, Lopes B, et al. Assessing ectasia susceptibility prior to LASIK: the role of age and residual stromal bed (RSB) in conjunction to Belin-Ambrósio deviation index (BAD-D). *Revista Brasileira de Oftalmologia*. 2014;73:75-80.
17. Schweitzer C, Roberts CJ, Mahmoud AM, Colin J, Maurice-Tison S, Kerautret J. Screening of forme fruste keratoconus with the Ocular Response Analyzer. *Invest Ophthalmol Vis Sci*. 2010;51:2403-2410.
18. Saad A, Gatinel D. Topographic and tomographic properties of forme fruste keratoconus corneas. *Invest Ophthalmol Vis Sci*. 2010;51:5546-5555.
19. Uçakhan ÖÖ, Cetinkor V, Özkan M, Kanpolat A. Evaluation of Scheimpflug imaging parameters in subclinical keratoconus, keratoconus, and normal eyes. *J Cataract Refract Surg*. 2011;37:1116-1124.
20. Bae GH, Kim JR, Kim CH, Lim DH, Chung ES, Chung TY. Corneal topographic and tomographic analysis of fellow eyes in unilateral keratoconus patients using Pentacam. *Am J Ophthalmol*. 2014;157:103-109.
21. Kozobolis V, Sideroudi H, Giarmoukakis A, Gkika M, Labiris G. Corneal biomechanical properties and anterior segment parameters in forme fruste keratoconus. *Eur J Ophthalmol*. 2012;22:920-930.
22. Ventura BV, Machado AP, Ambrósio R Jr, et al. Analysis of waveform-derived ORA parameters in early forms of keratoconus and normal corneas. *J Refract Surg*. 2013;29:637-643.
23. Piñero DP, Alió JL, Alesón A, Escaf Vergara M, Miranda M. Corneal volume, pachymetry, and correlation of anterior and posterior corneal shape in subclinical and different stages of clinical keratoconus. *J Cataract Refract Surg*. 2010;36:814-825.

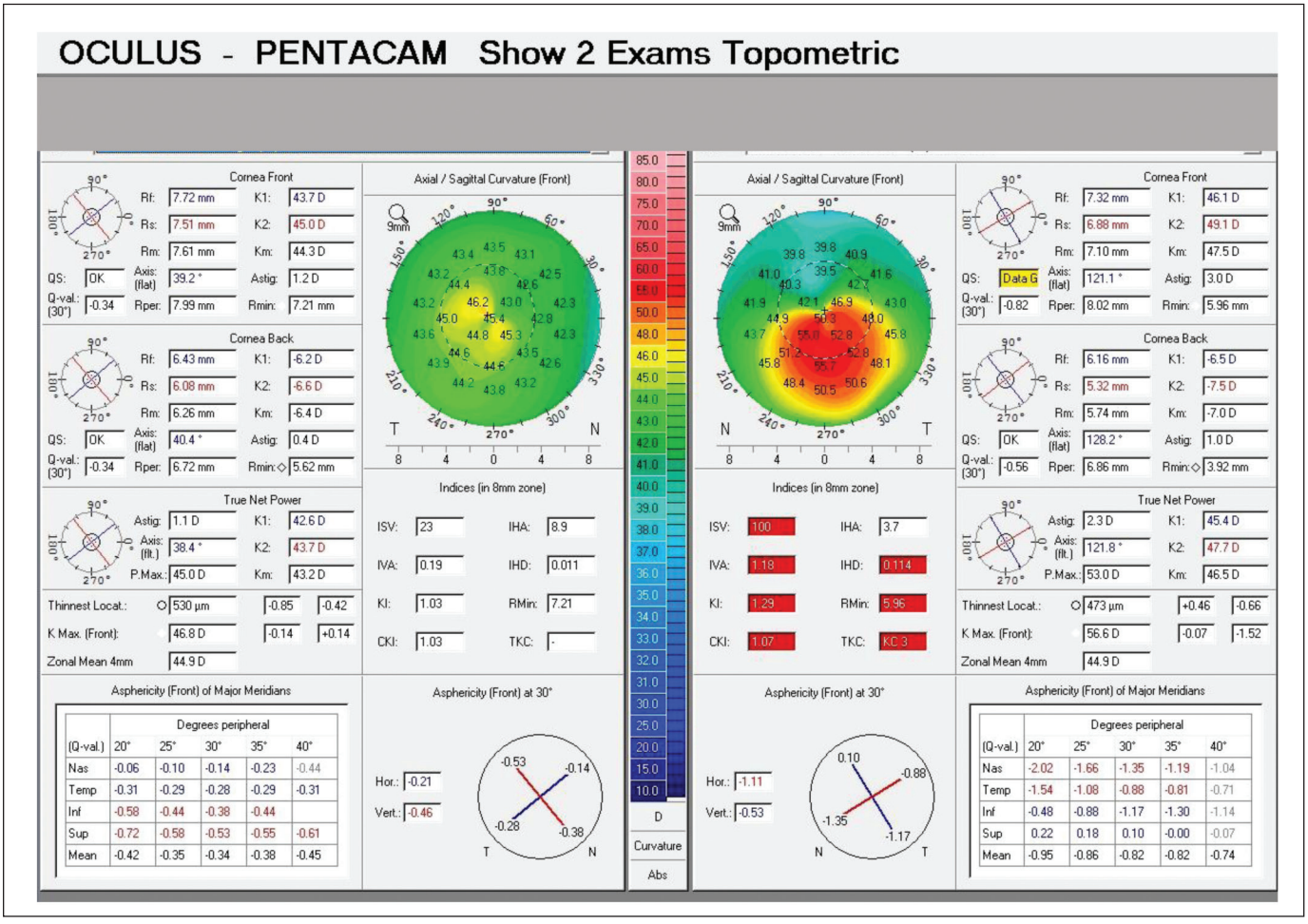

Figure A. Example of forme fruste keratoconus in the right eye.

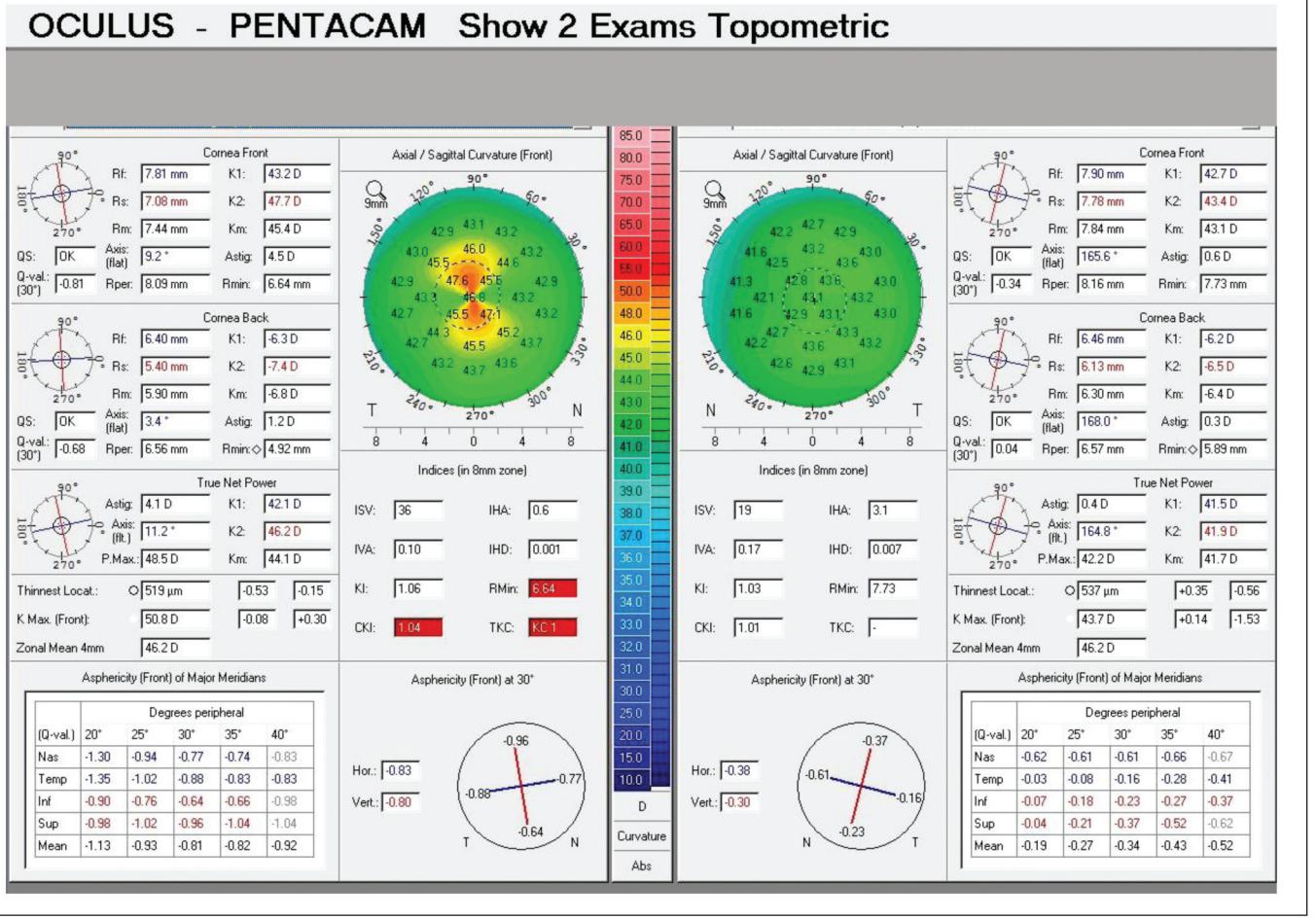

Figure B. Example of forme fruste keratoconus in the left eye.

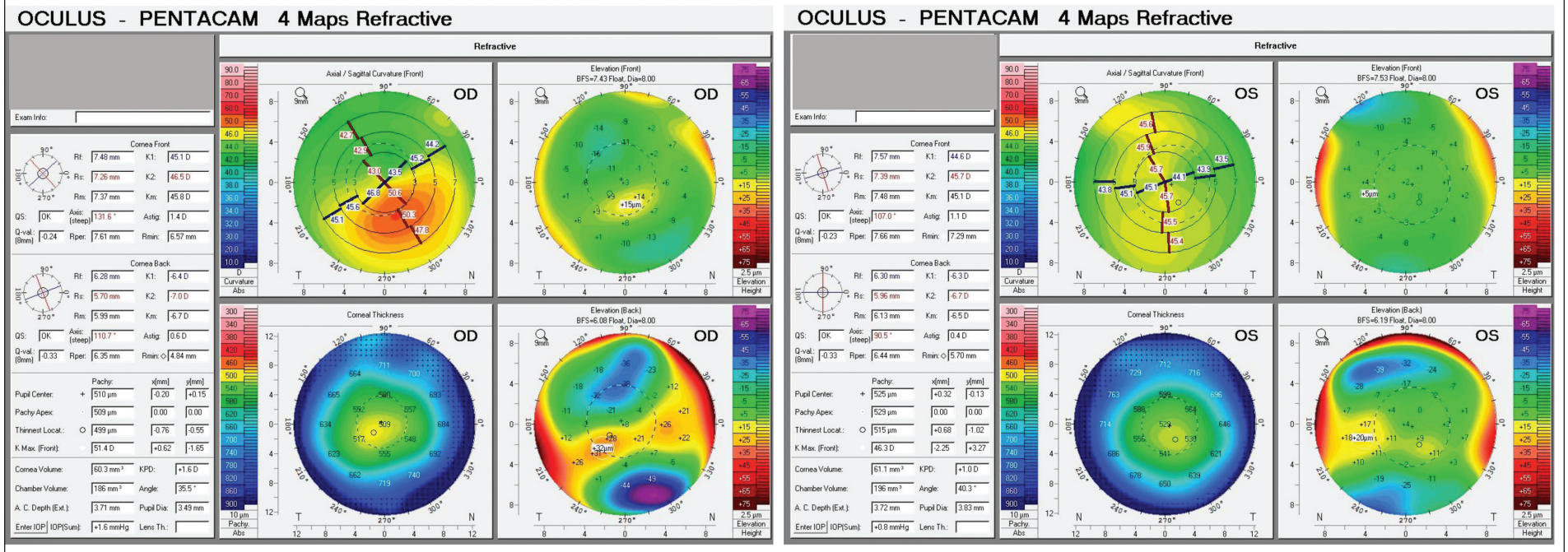

Figure C. Example of forme fruste keratoconus in the left eye.

TABLE A

Parameters From Corneal Tomography (Extracted From Oculus Pentacam HR)

Parameter	Operation Definition	Interpretation
ISV	Standard deviation of individual corneal sagittal radii from the mean curvature	Expression of the corneal surface irregularity
IVA	Measurement of the mean difference between superior and inferior corneal curvature	The value of curvature symmetry, similar to commonly used inferior/superior ratio
IHD	Decentration of elevation data in the vertical direction	Provides the degree of decentration in the vertical direction
Enhanced BFS front	Variable of the anterior corneal elevation	Enhanced anterior best fit sphere
Enhanced BFS back	Variable of the posterior corneal elevation	Enhanced back best fit sphere
Elevation B BFS Apex	Variable of the posterior corneal apex elevation	Best fit sphere posterior of the corneal apex
Elevation B BFS Thinnest	Variable of the posterior corneal thinnest point elevation	Best fit sphere posterior of the corneal thinnest point
Elevation B BFS Max 4-mm Zone	Variable of the posterior corneal elevation	Best fit sphere of the posterior cornea outside 4-mm zone from thinnest point
Elevation B BFTE Apex	Variable of the posterior corneal apex elevation	Best fit toric ellipsoid posterior of the corneal apex
Elevation B BFTE Thinnest	Variable of the posterior corneal thinnest point elevation	Best fit toric ellipsoid posterior of the thinnest point
Elevation B BFTE Max 4-mm Zone	Variable of the posterior corneal elevation	Best fit toric ellipsoid of the posterior cornea outside 4-mm zone from thinnest point
BAD-D	Belin/Ambrósio display	The D values represent the mean deviation, representing the pachymetric progression
ART Max	Ambrósio relational thickness maximum	Division of the thinnest point by the RPI Maximum
ART Average	Ambrósio relational thickness average	Division of the thinnest point by the RPI Average
RPI Max	Relative pachymetric index maximum	The value of pachymetric progression is calculated by reference to the average curve. For each meridian, a maximum value that expresses pachymetric progression is calculated.
RPI Average	Relative pachymetric index average	The value of pachymetric progression is calculated by reference to the average curve. For each meridian, a maximum value that expresses pachymetric progression is calculated.

ISV = index of surface variance; IVA = index of vertical asymmetry; IHD = index of height decentration
The Oculus Pentacam HR is manufactured by Oculus Optikgeräte, Wetzlar, Germany.

TABLE B

Variables Derived From the Signal of the Dynamic Bidirectional Applanation Device[a]

Variable	Operation Definition	Interpretation
Group 1		
A1	Peak intensity of first applanation event	Maximum surface area achieving planarity during inward deformation
A2	Peak intensity of second applanation event	Maximum surface area achieving planarity during recovery
Applanation peak difference	A2–A1	Difference in maximum planarity between inward and recovery phases
Concavity min	Minimum applanation intensity between A1 and A2	Depth and irregularity (nonplanarity) of deformation
Concavity mean	Mean applanation intensity between A1 and A2	Depth and irregularity of deformation average
Group 2		
Average P1P2	(P1+P2)/2	Average of the pressures at the 2 applanation events
Pmax	Peak value of pressure signal	Force and time required to reach first applanation event
Group 3		
Concavity duration	Time lapse between A1 and A2	Temporal delay of deformation recovery between applanation events
Concavity time	Time from onset of applied pressure to A1	Time required to achieve maximum deformation from onset of impulse
Lag time	Time between Pmax and concavity min	Delay between peak applied pressure and maximum deformation
Applanation onset time	Time from onset of applied pressure to A1	Time required to achieve first applanation from onset of impulse
Group 4		
Slope up	Positive slope of the first applanation peak, from inflection point to peak	Rate of achieving peak planarity
Slope down	Negative slope of the first applanation peak, from inflection point to peak	Rate of loss of peak planarity
Group 5		
Hysteresis loop area	Area enclosure by pressure vs applanation function	Hysteresis aggregated over entire deformation cycle except concavity
Group 6		
Impulse	Area under pressure vs time curve	Air pressure intensity

[a]*Data adapted from Hallahan KM, Sinha Roy A, Ambrósio R Jr, Salomao M, Dupps WJ Jr. Discriminant value of custom ocular response analyzer waveform derivatives in keratoconus.* Ophthalmology. *2014;121:459-468.*

TABLE C

Comparison of AUROC, Select Parameter Cut-off, Sensitivity, and Specificity for Variables Statistically Different Between Normal and FFKC Groups

Parameter	AUROC	SE[a]	*P*[b]	Sensibility	Specificity	Cut-off	CI 95%[c]
FECTB	0.953	0.0237	< .0001	85.71	98.68	> 0.4653	0.890 to 0.986
BAD-D	0.91	0.05	< .0001	90.48	82.89	> 0.96	0.835 to 0.959
B BFTE Th	0.872	0.05	< .0001	85.71	78.95	> 0	0.789 to 0.931
ART Maximum	0.863	0.06	< .0001	85.71	78.95	≤ 435	0.778 to 0.924
RPI Maximum	0.841	0.07	< .0001	80.95	97.37	> 1.29	0.753 to 0.907
B BFS Th	0.839	0.06	< .0001	85.71	75	> 3	0.751 to 0.906
ART Average	0.838	0.06	< .0001	80.95	75	≤ 557	0.749 to 0.905
RPI Average	0.836	0.06	< .0001	80.95	75	> 0.95	0.747 to 0.904
B BFTE 4Z	0.779	0.06	< .0001	71.43	67.11	> 7	0.684 to 0.857
p1area1	0.717	0.07	.0009	71.43	63.16	≤ 1,237.5	0.617 to 0.804
p1area	0.707	0.07	.0014	66.67	65.79	≤ 2,885.188	0.606 to 0.795
HLA	0.688	0.07	.0059	66.67	71.05	≤ 49.903	0.586 to 0.778
h1	0.663	0.07	.0213	61.9	68.42	≤ 319.688	0.560 to 0.756
h11	0.663	0.07	.0213	61.9	68.42	≤ 213.125	0.560 to 0.756
Impulse	0.650	0.07	.0323	66.67	67.11	≤ 4,401.975	0.546 to 0.744
dive1	0.649	0.07	.0297	61.90	63.16	≤ 279	0.545 to 0.743
Pmax	0.648	0.07	.0325	61.90	61.84	≤ 414	0.544 to 0.742
BFS Fr	0.646	0.07	.0267	61.90	63.16	≤ 7.86	0.542 to 0.740
B BFTE Ax	0.645	0.08	.0582	57.14	67.11	> -1	0.541 to 0.739
Ele B BFS 8-mm Apex	0.645	0.0764	.0582	57.14	67.11	> 1	0.541 to 0.739
uslope2	0.642	0.08	.0646	57.14	69.74	≤ 65.5	0.538 to 0.736
aspect2	0.630	0.0809	.1072	57.14	67.11	≤ 13.425	0.526 to 0.726
slew2	0.629	0.08	.1040	61.90	63.16	≤ 274.125	0.525 to 0.725
h2	0.629	0.0796	.1040	52.38	67.11	≤ 262.688	0.525 to 0.725
h21	0.629	0.0796	.1040	52.38	67.11	≤ 175.125	0.525 to 0.725
uslope1	0.627	0.0753	.0928	61.90	53.95	≤ 54.714	0.522 to 0.723
CRF	0.622	0.0742	.1012	61.90	68.42	≤ 8.9	0.517 to 0.718
dslope2	0.622	0.0830	.1432	52.38	69.74	≤ 16.732	0.517 to 0.718
mslew2	0.622	0.08	.1432	61.90	52.63	≤ 20.733	0.517 to 0.718
uslope21	0.622	0.0824	.1402	52.38	75.00	≤ 46.583	0.517 to 0.718
mslew1	0.622	0.0727	.0930	57.14	64.47	≤ 89	0.518 to 0.719
Aindex	0.620	0.0738	.1050	66.67	61.84	≤ 9.384	0.515 to 0.716
A1	0.617	0.0750	.1171	57.14	60.53	≤ 525	0.513 to 0.714
aspect21	0.617	0.0752	.1184	52.38	72.37	≤ 16.563	0.513 to 0.714
aspect1	0.614	0.0729	.1176	57.14	60.53	≤ 15.694	0.510 to 0.711
w2	0.613	0.0811	.1629	61.90	59.21	> 19	0.509 to 0.710
path1	0.610	0.0828	.1830	52.38	67.11	> 23.29	0.506 to 0.708
Enh BFS Back 8 mm	0.610	0.0689	.1094	61.90	61.84	≤ 6.49	0.506 to 0.708
CH	0.607	0.0766	.1633	57.14	51.32	≤ 9.9	0.502 to 0.705
dslope21	0.604	0.0740	.1598	61.90	52.63	≤ 30.65	0.500 to 0.702
Slope down	0.604	0.0742	.1609	57.14	57.89	> -92.74853801	0.500 to 0.702

TABLE C (cont'd)

Comparison of AUROC, Select Parameter Cut-off, Sensitivity, and Specificity for Variables Statistically Different Between Normal and FFKC Groups

Parameter	AUROC	SE[a]	*P*[b]	Sensibility	Specificity	Cut-off	CI 95%[c]
A2	0.601	0.0793	.2033	61.90	60.53	≤ 457	0.496 to 0.699
dslope1	0.599	0.0723	.1711	66.67	48.68	≤ 26.393	0.495 to 0.697
IHD	0.599	0.0663	.1369	57.14	67.11	> 5	0.494 to 0.697
p2area	0.597	0.0755	.1981	57.14	60.53	≤ 2,013	0.493 to 0.695
Aplhf	0.589	0.0702	.2035	57.14	61.84	> 1.3	0.485 to 0.688
Applanation onset time	0.588	0.0690	.2022	66.67	50.00	≤ 7.65	0.484 to 0.687
bindex	0.587	0.0764	.2545	52.38	59.21	≤ 9.656	0.483 to 0.686
Concavity min	0.586	0.0800	.2798	61.90	55.26	> 48.33333333	0.482 to 0.686
w11	0.585	0.0788	.2834	47.62	63.16	≤ 10	0.480 to 0.684
AvgP1P2	0.584	0.0725	.2486	57.14	51.32	≤ 172.5	0.479 to 0.683
Slope up	0.580	0.0779	.3070	61.90	44.74	≤ 77.84313725	0.475 to 0.679
Concavity mean	0.570	0.0831	.3982	52.38	57.89	≤ 113.0817204	0.466 to 0.670
p2area1	0.566	0.0730	.3631	57.14	55.26	≤ 884.5	0.462 to 0.667
path21	0.564	0.0721	.3756	61.90	47.37	≤ 35.025	0.459 to 0.664
w21	0.559	0.0738	.4275	57.14	44.74	> 8	0.454 to 0.659
slew1	0.558	0.0762	.4445	61.90	53.95	≤ 56.357	0.454 to 0.659
uslope11	0.557	0.0790	.4705	52.38	46.05	≤ 57	0.453 to 0.658
ISV	0.555	0.0669	.4149	61.90	52.63	≤ 19	0.450 to 0.655
Ele B BFS 8-mm max 4-mm zone	0.554	0.0746	.4729	52.38	59.21	> 13	0.449 to 0.655
dive2	0.554	0.0830	.5136	57.14	46.05	≤ 230.75	0.450 to 0.655
aspect11	0.540	0.0860	.6411	61.90	46.05	≤ 23.778	0.436 to 0.642
aspect11	0.540	0.0860	.6411	52.38	52.63	≤ 22.693	0.436 to 0.642
IVA	0.533	0.0718	.6467	47.62	51.32	≤ 0.16	0.429 to 0.635
w1	0.530	0.0735	.6822	61.90	51.32	≤ 21	0.426 to 0.632
Concavity time	0.529	0.0720	.6856	57.14	50.00	≤ 12.975	0.425 to 0.631
Lag time	0.522	0.0684	.7449	52.38	46.05	≤ .675	0.418 to 0.625
path2	0.505	0.0736	.9457	42.86	46.05	≤ 25.232	0.402 to 0.608
Applanation peak dif	0.505	0.0823	.9544	57.14	52.63	≤ -112	0.401 to 0.608
Concavity duration	0.501	0.0767	.9935	52.38	43.42	> 10.8	0.397 to 0.604
dslope11	0.501	0.0814	.9877	47.62	44.74	> 35.208	0.398 to 0.604

AUROC = area under the receiver operating characteristic curve; FFKC = forme fruste keratoconus; SE = standard error; CI = confidence interval; FECTB = function enhanced combined tomography and biomechanics; BAD-D = Belin/Ambrósio display; B BFTE Th = elevation B best fit toric ellipsoid thinnest; ART = Ambrósio relational thickness; RPI = relative pachymetric increase; B BFS Th = enhanced best fit sphere thinnest; B BFTE Ax = elevation B best fit toric ellipsoid apex; B BFTE 4Z = elevation B BFTE maximum 4-mm zone; HLA = hysteresis loop area; Pmax = pressure; BFS Fr = enhanced BFS front; CRF = corneal resistance factor; CH = corneal hysteresis; IHD = index of height decentration; ISV = index surface variation; IVA = index of vertical asymmetry

[a]*Data adapted from DeLong ER, DeLong DM, Clarke-Pearson DL. Comparing the areas under two or more correlated receiver operating characteristic curves: a nonparametric approach.* Biometrics. *1988;44:837-845.*

[b]*Area = 0.5.*

[c]*Binomial exact.*

TABLE D

Comparison of All ORA Variables

Parameter	Normal Group Mean ± SD (Range)	FFKC Group Mean ± SD (Range)	*P*[a]
p1area1	1,412.29 ± 447.54 (554.25 to 2,686.5)	1,085.19 ± 363.43 (553.5 to 1,762.38)	.0024[b]
p1area	3,331.25 ± 910.23 (1,402 to 5,606.06)	2,644.83 ± 746.93 (1,450.13 to 4,008)	.0037[b]
HLA	5,501.00 ± 15,339.15 (8,853 to 97,693)	43,614.55 ± 18,597.56 (-11,656.5 to 78,052)	.0086[b]
h1	377.05 ± 103.64 (218.62 to 640.87)	319.06 ± 102.74 (168.75 to 563.62)	.0228[b]
h11	251.37 ± 69.09 (145.75 to 427.25)	212.70 ± 68.49 (112.5 to 375 .35)	.0228[b]
Impulse	4,536.22 ± 323.30 (3,775.35 to 5,314.08)	4,402.86 ± 418.84 (3,796.58 to 5,807.36)	.0363
dive1	323.77 ± 117.79 (38.75 to 614.5)	266.39 ± 115.82 (19.5 to 561.75)	.0375
Pmax	423.74 ± 35.49 (344 to 505)	408.43 ± 45.09 (348 to 557)	.0391
mslew2	127.75 ± 56.57 (25.75 to 326)	97.08 ± 51.35 (19.25 to 173)	.0421
uslope2	85.99 ± 43.24 (14.67 to 239.12)	62.14 ± 45.55 (3.27 to 138.75)	.0478
slew2	86.40 ± 42.63 (17.5 to 239.12)	63.70 ± 44.10 (6.66 to 138.75)	.0487
aspect11	24.42 ± 9.85 (10.11 to 55.70)	25.29 ± 16.21 (9.37 to 75.15)	.5751
aspect2	18.15 ± 8.99 (4.62 to 55.02)	14.54 ± 11.03 (1.76 to 42.44)	.0685
h2	304.57 ± 90.38 (153.56 to 605.25)	252.13 ± 120.12 (72.18 to 466.87)	.0705
h21	203.04 ± 60.25 (102.37 to 403.5)	168.09 ± 80.08 (48.12 to 311.25)	.0705
uslope1	63.29 ± 31.77 (23.22 to 187.16)	49.71 ± 25.17 (18.13 to 112.35)	.0768
mslew1	106.28 ± 39.59 (53.5 to 239.5)	89.58 ± 30.31 (40.75 to 163.25)	.0876
CRF	9.75 ± 1.78 (6 to 148)	9.10 ± 1.99 (5 to 13.8)	.0893
dslope2	23.63 ± 12.93 (5.58 to 83.21)	19.51 ± 14.99 (2.58 to 57.71)	.0893
uslope21	68.73 ± 31.87 (13.91 to 157)	54.66 ± 42.13 (1.73 to 137.62)	.0893
Aindex	9.24 ± 1.05 (5.34 to 10)	8.59 ± 1.52 (4.95 to 10)	.0943
A1	582.36 ± 148.06 (358 to 916)	519.00 ± 160.57 (279 to 860)	.1005
aspect21	26.23 ± 14.16 (4.56 to 69.9)	20.85 ± 15.21 (2.18 to 62.25)	.1005
aspect1	17.98 ± 6.19 (8.33 to 39.31)	15.34 ± 6.19 (6.75 to 31.31)	.1109
w2	18.58 ± 4.57 (10 to 34)	22.67 ± 9.02 (11 to 42)	.1139
path1	22.45 ± 3.98 (15.29 to 36.43)	24.96 ± 6.05 (16.18 to 36.43)	.1232
CH	10.15 ± 1.62 (6.2 to 14.1)	9.27 ± 2.16 (6 to 13.1)	.1353
dslope21	40.85 ± 26.15 (5.79 to 135.12)	32.25 ± 24.35 (3.30 to 104.87)	.1459
Slope down	-105.20 ± 36.41 (-249.56 to -55.47)	-93.03 ± 38.26 (-181.99 to -40.32)	.1459
A2	476.96 ± 128.73 (256 to 807)	418.38 ± 174.69 (141 to 737)	.1585
dslope1	26.06 ± 8.89 (11.60 to 52.81)	23.25 ± 9.42 (9.85 to 45.1)	.1664
p2area	2,183.22 ± 550.90 (1,163.43 to 3,829.81)	1,928.98 ± 597.38 (447.5 to 2,909.63)	.1746
Aplhf	1.32 ± 0.31 (0.8 to 2.4)	1.55 ± 0.84 (0.9 to 5)	.212
Applanation onset time	7.69 ± 0 .43 (6.6 to 8.6)	7.66 ± 0.77 (6.75 to 10.65)	.2185
bindex	9.34 ± 1.08 (4.90 to 10)	8.42 ± 2.32 (1.80 to 10)	.2234
Concavity min	48.84 ± 9.88 (15.33 to 78.33)	51.87 ± 12.44 (23.66 to 167.33)	.2268
w11	11.00 ± 2.45 (5 to 17)	10.05 ± 3.25 (5 to 16)	.237
AvgP1P2	176.00 ± 22.23 (129 to 235.5)	179.43 ± 55.85 (140.5 to 411.5)	.2423
Slope up	76.83 ± 25.59 (33.70 to 148.92)	66.57 ± 30.08 (17.26 to 121)	.266
Concavity mean	119.83 ± 21.32 (81.88 to 185.03)	117.94 ± 44.04 (71.91 to 279.63)	.3266
p2area1	927.63 ± 274.63 (486 to 1,868)	831.18 ± 277.80 (206.5 to 1,316.5)	.3532
path21	36.04 ± 9.34 (14.58 to 66.56)	34.00 ± 8.43 (21.34 to 52.54)	.3716
w21	9.01 ± 3.05 (4 to 23)	10.67 ± 5.31 (5 to 24)	.4128
slew1	64.82 ± 31.25 (19.37 to 187.16)	56.41 ± 25.13 (19.5 to 112.35)	.4153
uslope11	62.02 ± 31.59 (14.5 to 181.37)	56.78 ± 31.67 (13.83 to 1,443.37)	.4254
dive2	235.69 ± 84.44 (87.5 to 551.25)	209.27 ± 111.58 (20 to 409)	.4487

TABLE D (cont'd)

Comparison of All ORA Variables

Parameter	Normal Group Mean ± SD (Range)	FFKC Group Mean ± SD (Range)	*P*[a]
aspect11	24.42 ± 9.85 (10.11 to 55.70)	25.29 ± 16.21 (9.37 to 75.15)	.5751
w1	21.57 ± 2.70 (15 to 28)	21.71 ± 3.51 (17 to 31)	.6742
Concavity time	12.92 ± 0.86 (10.42 to 14.62)	12.83 ± 0.87 (11.1 to 14.4)	.6838
Lag time	0.79 ± 0.55 (0.1 to 2.32)	0.74 ± 0.50 (0.075 to 2.25)	.7558
path2	25.61 ± 6.63 (11.57 to 51.14)	25.33 ± 6.05 (15.28 to 36.86)	.9441
Applanation peak dif	-105.39 ± 126.27 (-433 to 168)	-100.62 ± 169.75 (-353 to 199)	.9476
dslope11	40.62 ± 17.45 (14.10 to 104.06)	44.78 ± 27.95 (1,434 to 121.62)	.986
Concavity duration	10.91 ± 0.45 (9.9 to 12.15)	10.69 ± 1.14 (6.15 to 11.625)	.993

ORA = Ocular Response Analyzer (Reichert Ophthalmic Instruments, Depew, NY); SD = standard deviation; FFKC = forme fruste keratoconus; HLA = hysteresis loop area; Pmax = pressure; CRF = corneal resistance factor; CH = corneal hysteresis

[a]*Mann–Whitney* U *test.*

[b]*Statistically significant difference after Bonferroni correction.*